Interaction between Natural and Ventilated Cavitation around a Base Ventilated Hydrofoil

H. Zhou[1], M. Xiang[1], W. Zhang[1†], X. Xu[2], K. Zhao[3] and S. Zhao[1]

[1] *National University of Defense Technology, College of Aerospace Science and Engineering, Changsha, Hunan, 410073, China*
[2] *National Innovation Institute of Defense Technology, Beijing 100089, China*
[3] *Key Laboratory of Aerodynamic Noise Control, China Aerodynamics Research and Development Center, Mianyang, 621000, China*

†*Corresponding Author Email: zhangweihua@nudt.edu.cn*

ABSTRACT

In more recent years, supercavitation has attracted intensive attention due to its potentials in drag reduction for underwater vehicles. Ventilation is acknowledged as an efficient way to enhance cavitation when vehicles work under low speed. That means natural and ventilated cavitation may coexist in the flow and the interaction between the natural cavitation and ventilated cavitation has to be considered. In this paper, ventilated cavitating flow with natural cavitation around a base-ventilated hydrofoil is solved by a multi-phase cavitation solver based on OpenFOAM. The Partially-Averaged Navier-Stokes method is utilized for resolving turbulence. Lengths of the natural cavities are investigated under non-ventilation and ventilation conditions. Cavity shape evolution and interface deformation have also been studied under different angle of attack. Results show that ventilation cavitation at the base of the hydrofoil tends to depress the natural cavitation on the hydrofoil surface. As the increase of the attack angle, the shedding cavity of natural cavitation have a great impact on the interface shape of the ventilation cavity. Furthermore, the research also finds that the re-entry jet is the reason for natural cavitation shedding process and the interface deformation of the ventilated cavity arises from the vortex structures induced by the shedding natural cavitation.

Keywords: Natural cavitation; Ventilated cavitation; Interaction; PANS model; Numerical simulation; OpenFOAM.

NOMENCLATURE

A	conversion factor from mass to volume		p_v	vapor pressure
a_P	a function of velocity		P_u	production of the unsolved turbulence kinetic
C_c, C_v	coefficient for cavitation model		R	bubble radius
$C_{\varepsilon 1}, C_{\varepsilon 2}, C_{\varepsilon 2}^*$	dissipation coefficients for turbulence model		t	time
			U	velocity of fluid
C_μ	turbulence model coefficient		V	velocity of fluid
F	forces acting on the flow		α	volume fraction
f_k	unresolved-to-total ratios of turbulence kinetic		α_s	sum of volume fraction
			ε	turbulence dissipation
f_ε	unresolved-to-total ratios of turbulence dissipations		ε_u	unsolved turbulence dissipation
			μ	dynamic viscosity
$H(U)$	a matrix of velocity equation		ν	kinematic viscosity
k	turbulence kinetic		ρ	density of fluid
k_u	unsolved turbulence kinetic		$\sigma_k, \sigma_{ku}, \sigma_\varepsilon, \sigma_{\varepsilon u}$	Prandtl numbers for turbulence model
$\dot{m}$	mass transfer rate			
n_0	nuclei concentration		σ_v	vapour cavitation number
p	pressure of fluid		τ	Newtonian viscous stress tensor

1. INTRODUCTION

A lifting surface or hydrofoil operating in a liquid at high speed and at an angle of attack (AoA) to the oncoming flow is susceptible to cavitation occurrence, which usually results in the loss of performance and induces flow unsteadiness. In order to address this problem, Elms (1999) designed a base-ventilated hydrofoil for use in high-speed vessel, which is composed of a symmetric sub-cavitating foil section and a blunt tail section. Sometimes, however, cavitation numbers at which lift generating devices must operate are not sufficiently low to create supercavitation problems on hydrofoils. A classical strategy to address this problem is venting of incondensable gas about the hydrofoil to artificially induce supercavitation. To achieve this, Pearce (2011), Pearce and Brandner (2012a) designed a new base-ventilated hydrofoil, where the blunt tail section is replaced by an interceptor. Incondensable gas is supplied through the cavity ventilation manifold at the base of the hydrofoil.

Ji *et al.* (2010), Ji *et al.* (2010) adopted a three-component cavitation model to investigate the natural and ventilated cavitations around a super-cavitating test body, where the two types of cavitation almost happened at the same place. According to their research, we can find that the vapor cavity would be manageable by the gas ventilation. Jin *et al.* (2013) developed a code to analyze the supercavitation around a hemispherical cylinder with noncondensable gas and the movement of a free surface when an under-water object moves near it. The research confirmed that the speed of noncondensable gas had a great impact on the cavity stability and the free surface shape. Yu *et al.* (2015) investigated the cavitating turbulence flow with three components (water, vapor and air) around a cylinder vehicle. The evolution process of the natural and ventilated cavitation is studied. Results indicated that the vapor cavity could be rapidly depressed by the air injection. Jiang *et al.* (2017) also found that the air ventilation would impose restrictions on vapor generation in ventilated super-cavitating flow around an axisymmetric underwater body. Yang *et al.* (2018) conducted a series of numerical simulations around a two-dimensional NACA0015 hydrofoil, where the ventilated cavitation with three components (water, vapor and air) had been successfully predicted. Cavity shapes as well as the shedding frequency under different ventilation rates were also fully discussed. Yu *et al.* (2018) carried out both experiment and simulation on a NACA0015 hydrofoil with or without air injection. Results shows that air injection could alleviate the nature cavitation oscillation. Air cavities surrounded by the vapor sheet could promote vapor growth, resulting in an increase in the cavity shedding frequency. Karn *et al.* (2016) proposed that operation of a supercavitating underwater vehicle is driven by an interplay between the natural and ventilated supercavitation. Effect of these two distinct modes of supercavitation on each other during supercavity formation has been systematically discussed in their recent work (Karn

and Chawdhary (2018). Relative researches on natural and ventilated cavitation have been extensively studied in literatures (Salari *et al.* (2017), Shao *et al.* (2017), Barbaca *et al.* (2017), Barbaca *et al.* (2018)). However, most of these studies were focused on the cavity shape evolution process, interaction between the natural and ventilated cavitation are limited, especially when they formed at different locations.

In this study, the leading edge natural cavity and trailing edge ventilated cavity are investigated around a base-ventilated hydrofoil. A series of numerical simulations using the Partially-Averaged Navier-Stokes (PANS) turbulence model are carried out to explore the cavity evolution process, and interaction between the two types of cavitation is also discussed in detail.

2. MATHEMATICAL METHOD

In the current study, the multiphase flow is assumed incompressible, immiscible and in thermodynamic equilibrium, in which the relative motion between the phases can be neglected. Therefore, the homogeneous multiphase model and volume of fluid (VOF) approach are adopted for the multiphase cavitating flow simulation.

2.1 VOF Approach

In the VOF method the indicator function α represents the volume fraction which takes value 1 in one phase and 0 in the other. For a three-phase flow, given the phase fraction α, mixture properties of the system could be constructed as:

$$\rho = \alpha_l \rho_l + \alpha_v \rho_v + \alpha_g \rho_g \tag{1}$$

$$\mu = \alpha_l \mu_l + \alpha_v \mu_v + \alpha_g \mu_g \tag{2}$$

where ρ is the density, μ the dynamic viscosity. The subscript *l*, *v*, *g* represent the liquid, vapour and non-condensable gas respectively.

The basic form of transport equations for the volume fraction of each phase could write as:

$$\begin{cases} \dfrac{\partial(\alpha_l)}{\partial t} + \nabla.(\alpha_l U) = \dfrac{\dot{m}}{\rho_l} \\[2mm] \dfrac{\partial(\alpha_v)}{\partial t} + \nabla.(\alpha_v U) = -\dfrac{\dot{m}}{\rho_v} \\[2mm] \dfrac{\partial(\alpha_g)}{\partial t} + \nabla.(\alpha_g U) = 0 \end{cases} \tag{3}$$

where the $\dot{m}$ term on the RHS of the equations donates the mass transfer rate per unit volume caused by cavitation between the liquid and vapor phase.

Addition of all equations in Eq.3 leads to:

$$\nabla U = \left(\dfrac{1}{\rho_l} - \dfrac{1}{\rho_v} \right) \dot{m} \tag{4}$$

Adding and subtracting the $\alpha(\nabla U)$ term to the RHS of Eq.3 for each phase and utilizing Eq.4, the final form of the volume fraction equations can be expressed as

$$
\begin{cases}
\dfrac{\partial \alpha_l}{\partial t} + \nabla.(\alpha_l U) = \alpha_l (\nabla U) + A_l \dot{m} \\[2mm]
\dfrac{\partial \alpha_v}{\partial t} + \nabla.(\alpha_v U) = \alpha_v (\nabla U) - A_v \dot{m} \\[2mm]
\dfrac{\partial \alpha_g}{\partial t} + \nabla.(\alpha_g U) = \alpha_g (\nabla U) - A_g \dot{m}
\end{cases}
\tag{5}
$$

where A is the factor that converts the mass change rates to volumetric change rates, and $A_l = \dfrac{1}{\rho_l} - \alpha_l \left(\dfrac{1}{\rho_l} - \dfrac{1}{\rho_v} \right)$, $A_v = \dfrac{1}{\rho_v} + \alpha_v \left(\dfrac{1}{\rho_l} - \dfrac{1}{\rho_v} \right)$, $A_g = \alpha_g \left(\dfrac{1}{\rho_l} - \dfrac{1}{\rho_v} \right)$ for liquid, vapor and gas respectively.

2.2 Governing Equation

In the absence of relative motion the governing mass and momentum conservation equations for homogeneous mixture flow reduce to the single-phase form:

$$
\begin{cases}
\dfrac{\partial \rho}{\partial t} + \nabla.(\rho U) = 0 \\[2mm]
\dfrac{\partial (\rho U)}{\partial t} + \nabla.(\rho U \otimes U) = -\nabla p + \nabla.\tau + F
\end{cases}
\tag{6}
$$

where F stands for forces acting on the flow, such as surface tension force, gravity force and etc. τ represents the Newtonian viscous stress tensor.

Besides the momentum equation, a Poisson's equation for the pressure is constructed. According to Jasak (1996) and Demirdžić *et al*. (1993), the semi-discretised form of the momentum equation could be written as,

$$
U = \frac{H(U)}{a_p} - \frac{1}{a_p}\nabla p
\tag{7}
$$

where the $H(U)$ term consists of two parts: one is matrix coefficients for all neighbours multiplied by corresponding velocities, and the other part is the source part including the source part of the transient term and all other source terms apart from the pressure gradient.

Combining with the velocity divergence term in Eq. (4), the final form of the pressure equation is given as,

$$
\nabla.\left(\frac{H(U)}{a_p} \right) - \nabla.\left(\frac{1}{a_p}\nabla p \right) = \left(\frac{1}{\rho_l} - \frac{1}{\rho_v} \right)\dot{m}
\tag{8}
$$

Finally, the $p-U$ coupling is solved by the PIMPLE loop in the current study.

2.3 Cavitation Model

Cavitation model is used to determine the mass transfer rate between the cavitation phase pair. It acts as a source term in the phase volume fraction equations and may also affect the momentum and pressure Poisson equation. In this study, the Schnerr model (Schnerr and Sauer (2001)) is adopted.

According to the work of Schnerr and Sauer, if the system pressure is sufficiently low and the pressure difference $p_v - p_\infty$ is large, the Rayleigh relation could be considered as an adequate description for the bubble growth:

$$
\frac{dR}{dt} = \sqrt{\frac{2}{3}\frac{p_\infty - p_v}{\rho_l}}
\tag{9}
$$

And with respect to cavitation, the vapour volume fraction α_v may be reformulated as follows:

$$
\alpha_v = \frac{V_v}{V_{cell}} = \frac{n_0 \cdot \frac{4}{3}\pi R^3}{1 + n_0 \cdot \frac{4}{3}\pi R^3}
\tag{10}
$$

Based on Eq.9 and Eq.10, relation between the bubble growth and volume fraction change rate can be formulated, and the final form of Schnerr-Sauer cavitation model is

$$
\begin{cases}
\dot{m}^+ = C_c \dfrac{\rho_v \rho_l}{\rho} \alpha_v (1 - \alpha_v) \dfrac{3}{R} \sqrt{\dfrac{2}{3}\dfrac{p - p_v}{\rho_l}} & p > p_v \\[4mm]
\dot{m}^- = C_v \dfrac{\rho_v \rho_l}{\rho} \alpha_v (1 - \alpha_v) \dfrac{3}{R} \sqrt{\dfrac{2}{3}\dfrac{p_v - p}{\rho_l}} & p < p_v
\end{cases}
\tag{11}
$$

2.4 Turbulence Model

Since cavitation is generally considered as a high turbulent phenomenon (laberteaux and Ceccio (2001a), laberteaux and Ceccio (2001b), Iyer and Ceccio (2002)). Turbulence modeling plays a key role and must also be addressed adequately in addition to the cavitation model. The RANS approach has been popular for engineering turbulent flow computations, such as the standard $k - \varepsilon$ model. However, it has also been repeatedly reported that the RANS methods are unable to predict unsteady cavitation due to an over estimation of turbulence viscosity around the cavity closure. In the current study, the Partially-Averaged Navier-Stokes (PANS) method, which is proposed by Girimaji (2006), are utilized. The objective of PANS, like hybrid models, is to resolve large scale structures at reasonable computational expense. It can also be considered as filter-based turbulence model, whose filter width is mainly controlled by the ratio of unsolved-to-total kinetic energy f_k and unresolved-to-total dissipation f_ε, which are defined as:

$$
f_k = \frac{k_u}{k}, \quad f_\varepsilon = \frac{\varepsilon_u}{\varepsilon}
\tag{12}
$$

where the subscript u stands for the unsolved turbulence quantities.

Transport equations of the unsolved turbulence kinetic energy and dissipation rate of the $k - \varepsilon$ PANS model are shown in the following equations:

$$\begin{cases} \dfrac{\partial k_u}{\partial t} + U_i \dfrac{\partial k_u}{\partial x_i} = P_u - \varepsilon_u \\[3mm] \qquad\qquad + \dfrac{\partial}{\partial x_i}\left[\left(\nu + \dfrac{\nu_u}{\sigma_{ku}}\right)\dfrac{\partial k_u}{\partial x_j}\right] \\[5mm] \dfrac{\partial \varepsilon_u}{\partial t} + U_i \dfrac{\partial \varepsilon_u}{\partial x_i} = C_{\varepsilon 1} P_u \dfrac{\varepsilon_u}{k_u} - C_{\varepsilon 2}^* \dfrac{\varepsilon_u^2}{k_u} \\[5mm] \qquad\qquad + \dfrac{\partial}{\partial x_i}\left[\left(\nu + \dfrac{\nu_u}{\sigma_{\varepsilon u}}\right)\dfrac{\partial \varepsilon_u}{\partial x_j}\right] \end{cases} \quad (13)$$

where P_u is the production of the unsolved turbulence kinetic k_u. Compared with the standard RANS $k - \varepsilon$ model, the dissipation coefficient and Prandtl number were modified as,

$$\begin{cases} C_{\varepsilon 2}^* = C_{\varepsilon 1} + \dfrac{f_k}{f_\varepsilon}\left(C_{\varepsilon 2} - C_{\varepsilon 1}\right) \\[4mm] \sigma_{ku} \equiv \sigma_k \dfrac{f_k^2}{f_\varepsilon}, \quad \sigma_{\varepsilon u} \equiv \sigma_\varepsilon \dfrac{f_k^2}{f_\varepsilon} \end{cases} \quad (14)$$

Eventually turbulence viscosity defined by $k - \varepsilon$ PANS models has the form:

$$\nu_u = C_\mu \frac{k_u^2}{\varepsilon_u} \quad (15)$$

The PANS model is a bridging model. By changing the value of f_k, it can switch from RANS ($f_k = 1$) to DNS($f_k = 0$) smoothly. Since it can significantly reduce the eddy viscosity and generate much stronger time-dependency compared with the standard $k - \varepsilon$ model, PANS model has been extensively used in unsteady cavitating flow simulations (Huang and Wang (2011), Hu *et al.* (2014), Shi *et al.*(2014), Huang *et al.* (2017)).

3.   CASE SETUP

Numerical simulations are carried out based on the base-ventilated hydrofoil design by Pearce (2011), Pearce and Brandner (2012a). A brief schematic diagram of the hydrofoil is illustrated in Fig.1. An artificially induced trailing supercavity is formed from base of the hydrofoil. Due to the flow asymmetry, caused by the steps with detached cavity surfaces, lift is consequently produced at zero incidence. Leading edge partial vaporous cavitation also can be found with incidence increases. Since natural cavity and ventilated cavity coexist on the hydrofoil surface, interaction between them should be fully discussed.

Computation domain and boundary conditions of the simulations are shown in Fig.2. An inlet condition is set with values of free stream velocity components and turbulence quantities on the left-inlet side. On the right-exit side of the domain a pressure outlet condition with a fixed static pressuer is imposed. The inflow velocity is set to $U_\infty = 10\, m/s$, vapour cavitation number is $\sigma_v = (p - p_v)/\frac{1}{2}\rho U_\infty^2 = 0.75$ for cavitating condition, and the static pressure is adjusted to vary with the cavitation number. The ventilation flow rate is given as a mass flow rate, $Q_m = 200$, in Standard Litres per Minute(SLPM). Detailed geometry definition of the hydrofoil and flow condition parameters could refer to the work of Pearce and Brandner (2012b).
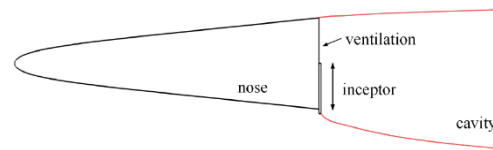
Fig. 1. Concept of base-ventilated hydrofoil.
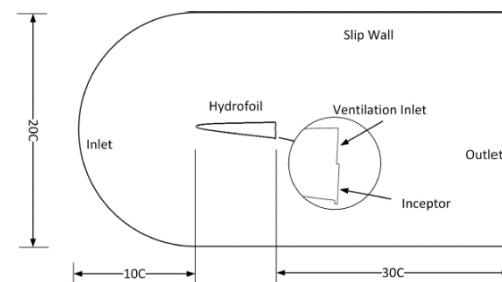
Fig. 2. Computational domain of the base-ventilated hydrofoil.

There are three different wall-function grids for each type of resolution (coarse, medium, fine) from y^+ values of 30, 60 and 90. Pressure coefficients on the hydrofoil surface are selected as a indication for gaging mesh convergence, and some results are shown in Fig.3. Finally, the medium mesh with $y^+ = 30$ is selected.
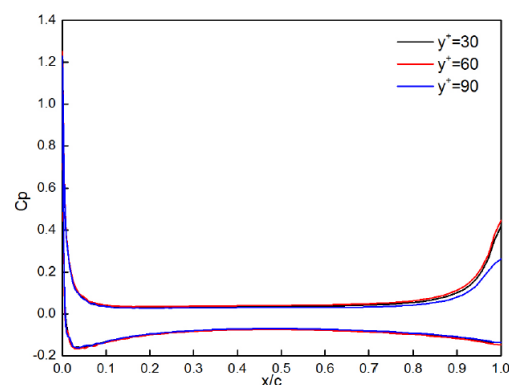
Fig. 3. Mesh convergence check for different y^+ values (medium mesh).
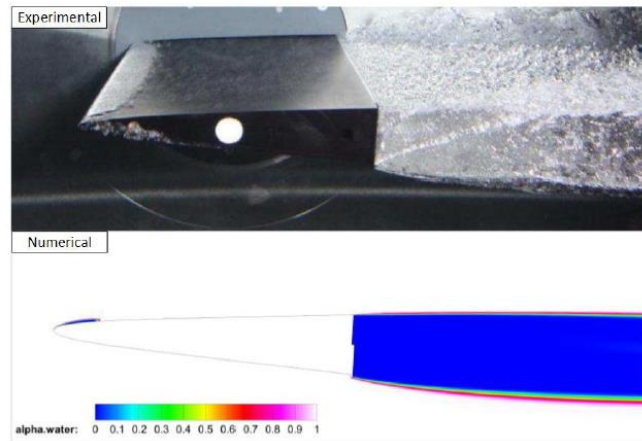
(a) AoA=2.75°
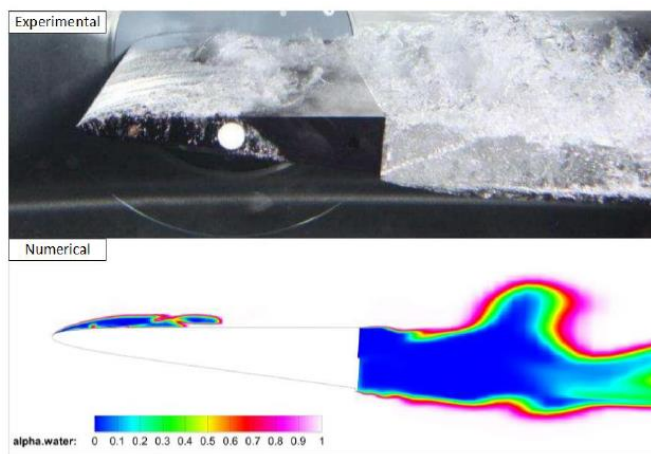
(b) AoA=4°

Fig. 4. Comparison of the numerical and experimental results.

Furthermore, validations are carried out under natural cavitation with ventilation condition. The incidences of the foil in the validation cases are AoA=2.75° and 4°. Comparison of the numerical results and experimental pictures are presented in Fig.4(a) and Fig.4(b). Errors of the leading edge natural cavity length between the numerical and experimental results are 1.6% and 3.4% chord length respectively. The simulated cavity shapes also match well with those from experiments. It suggests that the solver has a good performance in natural and ventilated cavitating flow prediction.

4. RESULTS AND DISCUSSION

When at low or moderate angle of attack conditions, there might form two separate cavities on the suction side of the base-ventilated hydrofoil. One is a natural cavity located at leading edge, the other is a ventilated cavity located at the base of the hydrofoil. While at large attack angle conditions, the leading edge natural cavity may merge with the ventilated cavity. Interaction between the natural and ventilated cavity is the product which these two types of cavitation gamble mutually.

In this section, influence of these two types of cavitation on each other under different flow conditions will be discussed, and the mechanism behind them will also be fully explored.

4.1 Influence of Gas Ventilation on Natural Cavitation

In order to obtain relatively steady and time-averaged results, ratios of unsolved-to-total kinetic energy and dissipation $f_k = 1$, $f_\varepsilon = 1$ are chosen for cases in this sub-section. Vapor volume faction distributions of the leading edge natural cavitation under different simulation conditions are shown in Fig.5 and Fig.6. The simulated results show that lengths of the leading edge natural cavity in cases with gas ventilation are shorter than those in cases without gas ventilation. It may be hypothesized that the gas ventilation at the base of the hydrofoil would impose restrictions on the leading edge natural cavity generation.

To illustrate this assumption, the pressure distributions near the hydrofoil are further studied, as shown in Fig.7 and Fig.8. According to the given results, we can find that the ventilated gas pressure is much higher than the saturated vapor pressure.
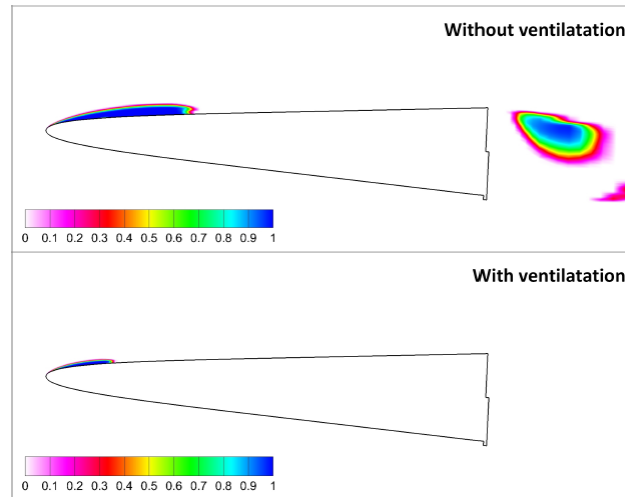
Fig. 5. Vapor volume fraction distribution around the hydrofoil (AoA=2.75).
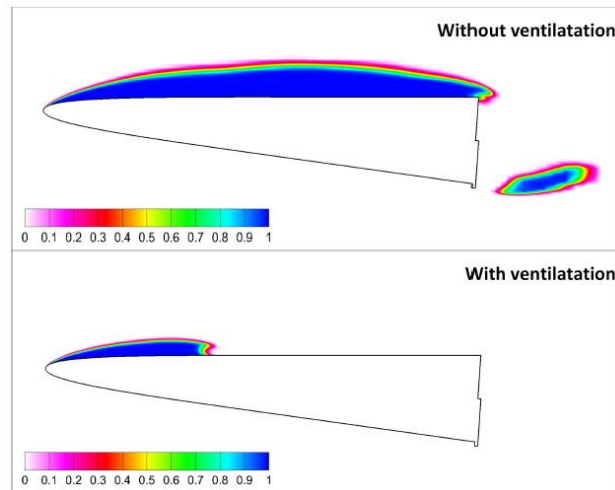
Fig. 6. Vapor volume fraction distribution around the hydrofoil ($AoA = 4^o$).

Presence of the gas ventilation causes a rise of the pressure at the base of the hydrofoil, and in turn affect the pressure on the suction side of the hydrofoil, resulting in smaller low pressure area and leading edge vapor cavity length.

Based on the discussion above, we could ascertain that the gas ventilation at the base of the hydrofoil depress the leading edge natural cavitation by changing the pressure distribution on the suction side of the hydrofoil.

4.2 Influence of Natural Cavitation on Ventilated Cavity

To illustrate the influence of the natural cavitation on the ventilated cavity, the evolution process of the cavity shape need to be investigated. Therefore, a series of unsteady multiphase cavitation simulations have to be carried out. Considering that the leading edge natural cavitation is usually unsteady flow, ratios of unsolved-to-total kinetic energy and dissipation should be set as $f_k = 0.2, f_\varepsilon = 1$.

In order to clearly represent the volume fraction distribution for all of the three phases, we define a new field scaler as follows,

$$\alpha_s = \alpha_v + 2\alpha_g \qquad (16)$$

In Eq.16, if there is only water in a control volume, then $\alpha_s = 0$; if there is only vapor, $\alpha_s = 1$ and if there is only gas, $\alpha_s = 2$. Values between 0 and 1 or 1 and 2 stand for mixture of two or three phases. Distributions of the volume fraction for the whole three phases with gas ventilation under different angle of attack, which indicate the evolution of natural and ventilated cavities, are shown in Fig.9 to Fig.12.

According to the given results in Fig.9, we can find that scale of the leading edge natural cavity, which is in yellow color, is relatively small under small angle of attack (e.g., AoA=2.75^o).The shedding cavities are less intense and far from the ventilated cavity, which is in white color located at the base of the
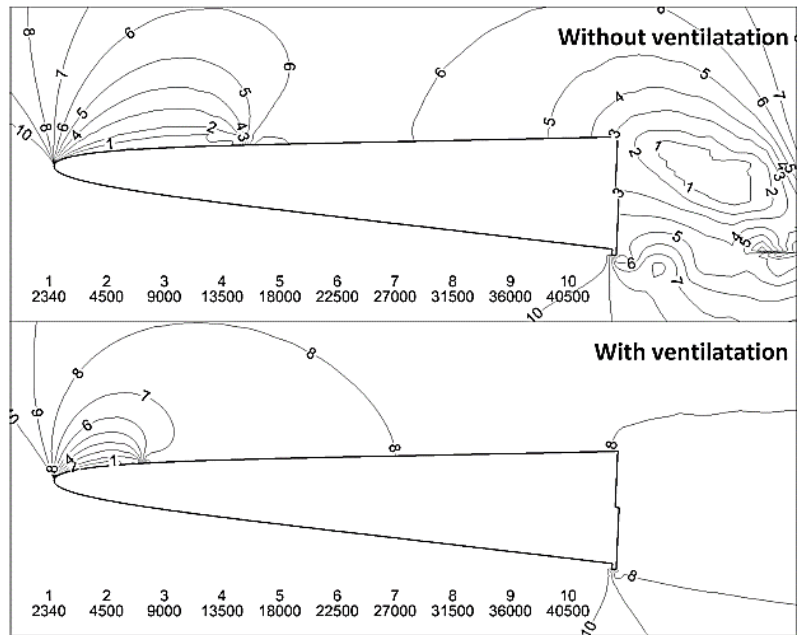
Fig. 7. Pressure distribution around the hydrofoil (AoA = 2.75^o).
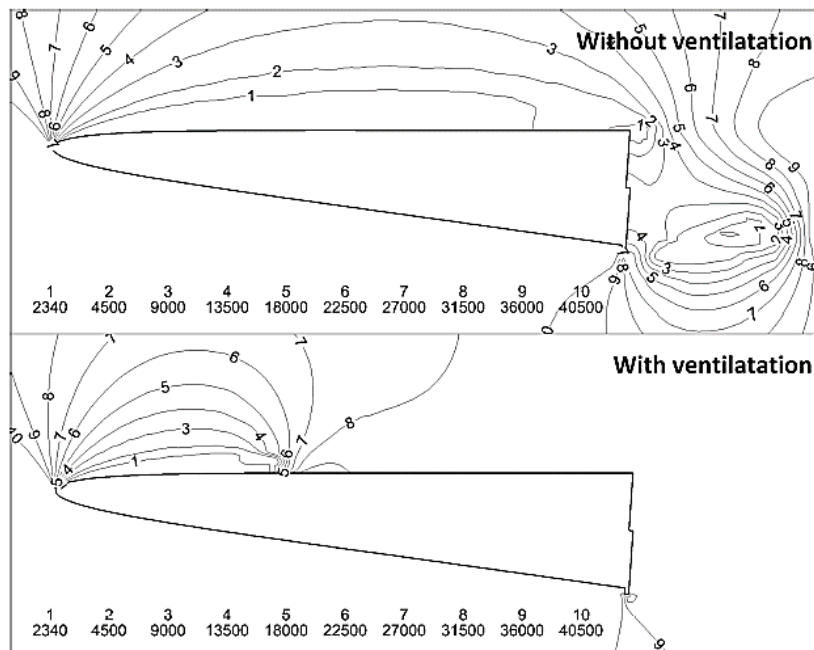
Fig. 8. Pressure distribution around the hydrofoil (AoA = 4°).

hydrofoil. So the ventilated cavity is free from the impact of the leading edge natural cavitation.

While under moderate attack angle (e.g. AoA=4°), the leading edge natural cavity scale becomes larger and the shedding cavities are more powerful. These shedding cavities per se are in low pressure, and when they move close to the ventilated cavity, significant periodic deformation of the ventilated cavity interface could be observed, as shown in Fig.10.

In cases where the angle of attack is much larger (e.g., AoA=6°) that the leading edge natural cavity could reach the base of the hydrofoil, air in the ventilated cavity would move upstream, encountering the natural cavity, and push it back to the leading edge. However, the angle of attack is still not large enough that the forward moved ventilated cavity could attach on the leading edge stably. Almost immediately when it reaches the leading edge, the ventilated cavity will shed off and return to the base of the hydrofoil, and then begin a new
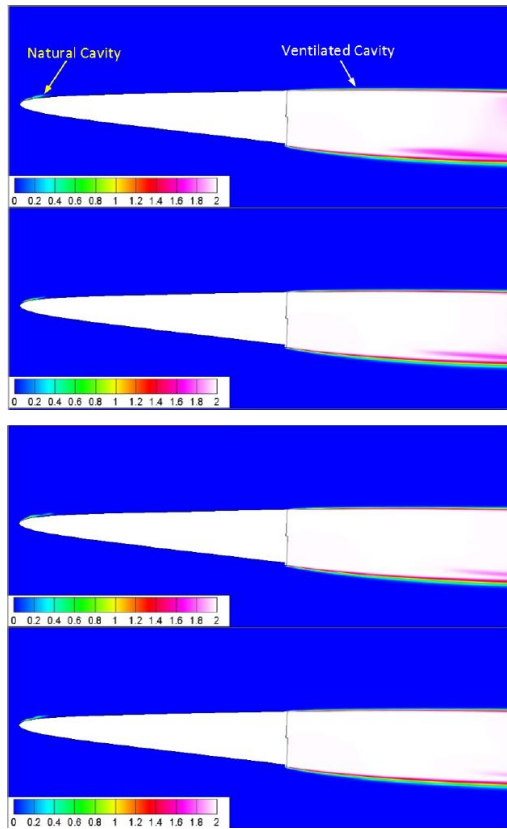
Fig. 9. Evolution of the cavity shape
(AoA = 2.75^o).
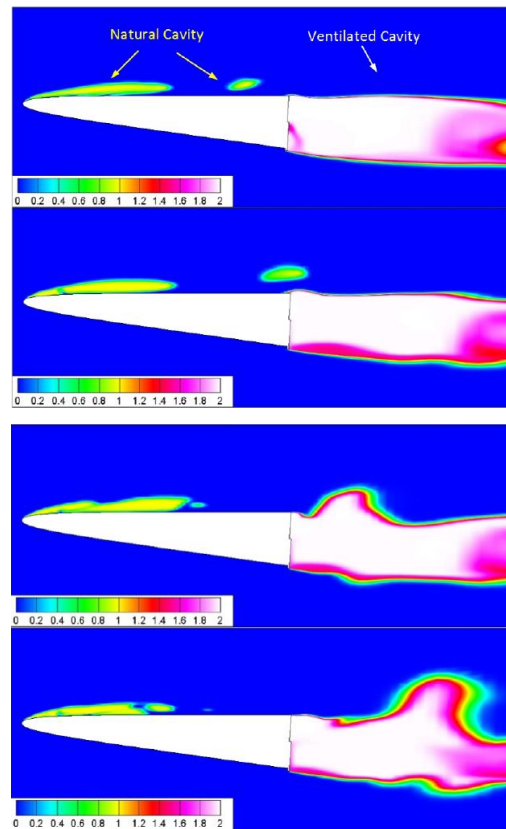
Fig. 10. Evolution of the cavity shape
(AoA = 4°).

forward movement cycle. Cavity shape evolution under AoA=6° is shown in Fig.11.

If the angle of attack is larger enough (e.g., AoA=8°), pressure near the lee side of the hydrofoil maintains at a relatively low level, then the forward moved ventilated cavity would move upstream. After a limited rounds of game with the leading edge natural cavitation, the ventilated cavity finally attach on the leading edge stably, forming a ventilated supercavity on the suction side of the hydrofoil, as shown in Fig.12.

In summary, the ventilated cavity at the base of the hydrofoil would depress the leading edge natural cavity both in separated and merged situations. This is caused by the rise of the pressure around the hydrofoil due to gas ventilation. In the case of separated natural and ventilated cavities, the ventilated cavity is almost free from the leading edge cavity under low angle of attack. However, under moderate attack angles, significant interface deformation of the ventilated cavity could be observed, which has great relation with the natural cavity shedding process. While in the case of merged natural and ventilated cavities, upstream movements of the ventilated cavity appear on the suction side of the hydrofoil. This behavior is mainly driven by the pressure difference induced by the large scale natural cavity under large attack angle.

4.3 Deformation Mechanism Analysis of the Ventilated Cavity

In the previous sub-sections, impacts of the leading edge natural cavity and base-ventilated cavity on each other have been discussed. A new phenomenon that the natural cavity might cause interface deformation of the ventilated cavity has been found based on the above analysis. In this part, taking the moderate attack angle case (AoA=4°) as an example, the flow quantities will be analysed to explain the mechanism for interface deformation. As shown in Fig.13, combine the stream lines and volume fraction distribution around the leading edge, we can find that locations of the re-entry jets are the same those where the cavity is sheared off. Therefor a conclusion that the re-entry jets are the main cause for leading edge natural cavitation shedding could be made.

Furthermore, the velocity disturbance caused by the natural cavitation and ventilation is evaluated by subtracting the free stream velocity vector from the cavitating flow vector and is shown in Fig.14. As the top figure indicated, shedding cavity is always accompanied by vortex structures. When the shedding cavity as well as the vortex structure reach to the base of the hydrofoil, an initial interface deformation of the ventilated cavity happens under the shearing effect of the first vortex, as shown in the bottom figure of Fig.14. As the flow developing
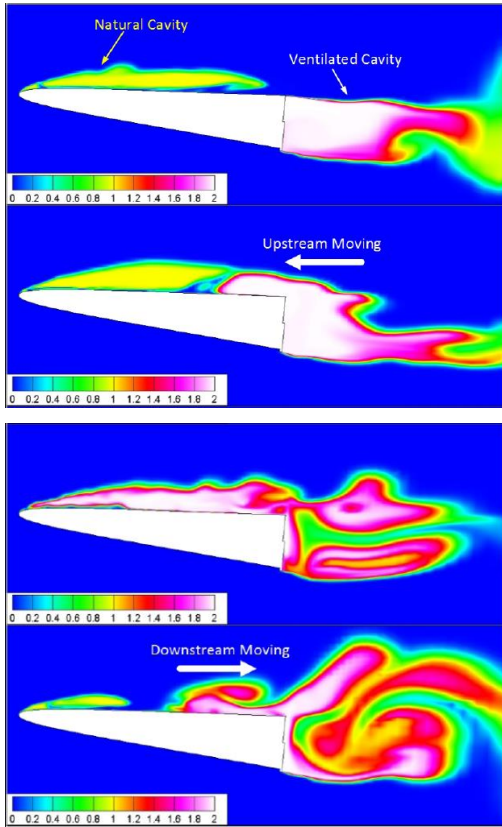
Fig. 11. Evolution of the cavity shape

($\text{AoA} = 6^{\text{o}}$).
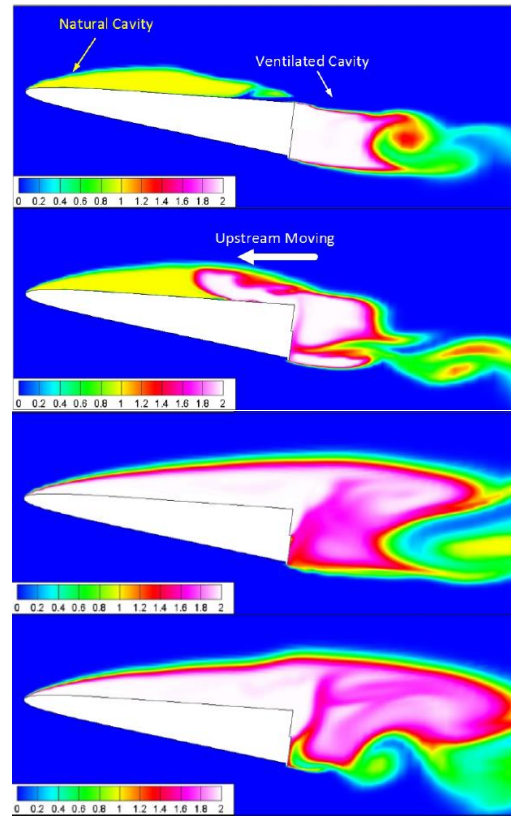
Fig. 12. Evolution of the cavity shape

($\text{AoA} = 8^{\text{o}}$).
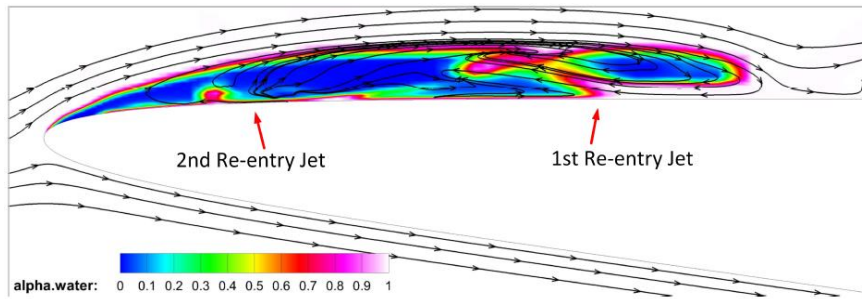
Fig. 13. Stream lines at the leading edge of the hydrofoil (AoA=4°).
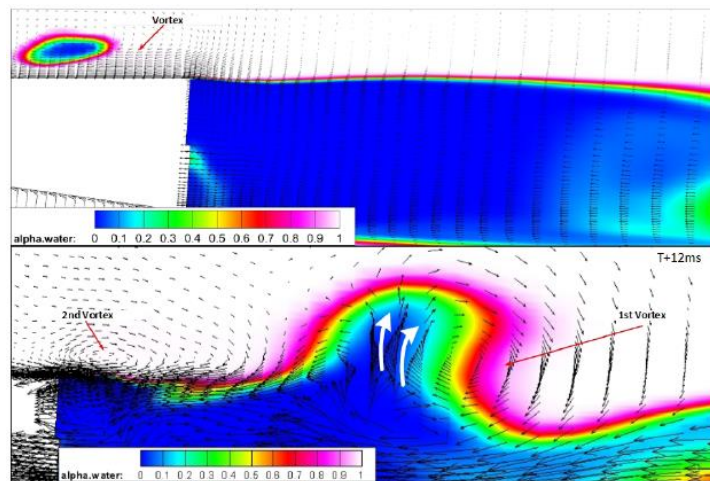
Fig. 14. Relative velocity vector and water volume fraction distribution ($\text{AoA} = 4^{\text{o}}$).

downstream, the vortex becomes more powerful. Under the impact of the second vortex, the interface is rushed up and then scrolled down, suffering a significant deformation, as shown in the bottom figure of Fig.14.

In summary, the natural cavitation shedding is caused by the re-entry jets at the wake of the cavity and the interface deformation of the ventilated cavity arises from the vortex structures near the interface induced by natural cavitation shedding process.

5. CONCLUSION

In this study, the interaction between natural and ventilated cavitation on a base-ventilated hydrofoil is investigated using a multiphase cavitation solver which couples with PANS turbulence model in OpenFOAM plartform. Results of natural cavities lengths and pressure distribution suggest that ventilation cavity tends to depress the natural cavity. The transient cavity evolution process was carefully investigated which showed that the shedding cavity of natural cavitation have a great impact on the interface shape of the ventilation cavity. Furthermore, the research also found that the re-entry jet is the reason for natural cavitation shedding process and the interface deformation of the ventilated cavity arises from the vortex structures induced by the shedding natural cavitation.

ACKNOWLEDGMENTS

REFERENCES

Barbaca, L., B. W. Pearce and P. A. Brandner (2017). Experimental study of ventilated cavity flow over a 3-d wall-mounted fence. *International Journal of Multiphase Flow* 97, 10 – 22.

Barbaca, L., B. W. Pearce and P. A. Brandner (2018). An experimental study of cavity flow over a 2-d wall-mounted fence in a variable boundary layer. *International Journal of Multiphase Flow* 105, 234 – 249.

Demirdžić, I., Ž. Lilek and M. Perić (1993). A collocated finite volume method for predicting flows at all speeds. *International Journal for Numerical Methods in Fluids* 16(12), 1029–1050.

Elms, A. R. (1999). Improved hydrofoil device. International Patent WO 99/57007, World Intellectual Property Organisation.

Girimaji, S. S. (2006). Partially-Averaged Navier-Stokes Model for Turbulence: A Reynolds-Averaged Navier-Stokes to Direct Numerical Simulation Bridging Method. *Journal of Applied Mechanics* 73(3), 413.

Hu, C. L., G. Y. Wang, G. H. Chen and B. Huang (2014). A modified PANS model for computations of unsteady turbulence cavitating flows. *Science China: Physics, Mechanics and Astronomy* 57(10), 1967–1976.

Huang, B. and G. Y. Wang (2011). Partially Averaged Navier-Stokes method for time-dependent turbulent cavitating flows. *Journal of Hydrodynamics* 23(1), 26–33.

Huang, R., X. Luo and B. Ji (2017). Numerical simulation of the transient cavitating turbulent flows around the Clark-Y hydrofoil using modified partially averaged Navier-Stokes method. *Journal of Mechanical Science and Technology* 31(6), 2849–2859.

Iyer, C. O. and S. L. Ceccio (2002). The influence of developed cavitation on the flow of a turbulent shear layer. *Physics of Fluids* 14(10), 3414–3431.

Jasak, H. (1996). Error Analysis and Estimation for the Finite Volume Method with Applications to Fluid Flows. Phd thesis, University of London Imperial College, London, United Kingdom.

Ji, B., X. W. Luo, X. X. Peng, Y. Zhang, Y. L. Wu and H. Y. Xu (2010). Numerical investigation of the ventilated cavitating flow around an under-water vehicle based on a three-component cavitation model. *Journal of Hydrodynamics* 22(6), 753–759.

Ji, B., X. W. Luo, Y. Zhang, H. J. Ran, H. Y. X-u and Y. L. Wu (2010). A three-component model suitable for natural and ventilated cavitation. *Chinese Physics Letters* 27(9).

Jiang, C. X., S. L. Li, F. C. Li, and W. Y. Li (2017). Numerical study on axisymmetric ventilated supercavitation influenced by drag-reduction additives. *International Journal of Heat and Mass Transfer* 115, 62–76.

Jin, M.-S., C.-T. Ha and W.-G. Park (2013). Numerical study of ventilated cavitating flows with free surface effects. *Journal of Mechanical Science and Technology* 27(12).

Karn, A. and S. Chawdhary (2018). On the synergistic interrelation between supercavity formation through vaporous and ventilated routes. *International Journal of Multiphase Flow* 104, 1 – 8.

Karn, A., R. E. Arndt and J. Hong (2016). Gas entrainment behaviors in the formation and collapse of a ventilated supercavity. *Experimental Thermal and Fluid Science* 79, 294 –300.

Laberteaux, K. R. and S. L. Ceccio (2001a). Partial cavity flows. part 1. cavities forming on models without spanwise variation. *Journal of Fluid Mechanics* 431, 141.

Laberteaux, K. R. and S. L. Ceccio (2001b). Partial cavity flows. part 2. cavities forming on test objects with spanwise variation. *Journal of Fluid Mechanics* 431, 4363.

Pearce, B. W. (2011). Ventilated Supercavitating Hydrofoils for Ride Control of High-Speed Craft. phdthesis, University of Tasmania, Tasmania, Australia.

Pearce, B. W. and P. A. Brandner (2012a). Experimental Investigation of A Base-Ventilated Supercavitating Hydrofoil with Interceptor. In Proceedings of the 8th International Symposium on Cavitation, Singapore.

Pearce, B. W. and P. A. Brandner (2012b). The Effect of Vapour Cavitation Occurrence on the Hydrodynamic Perfoermance of An Intercepted Base-Ventilated Hydrofoil. In *Proceedings of the 18th Australasian Fluid Mechanics Conference*, Launceston, Australia.

Salari, M., S. M. Javadpour and S. Farahat (2017). Experimental study of fluid flow characteristics around conical cavitators with natural and ventilated cavitations. *Journal of Marine Science and Technology* 25, 489 – 498.

Schnerr, G. H. and J. Sauer (2001). Physical and numerical modeling of unsteady cavitation dynamics. In *Proceedings of the 4th International Conference on Multiphase Flow*, New Orleans, La, USA.

Shao, S., A. Karn, B. K. Ahn, R. E. Arndt and J. Hong (2017). A comparative study of natural and ventilated supercavitation across two closed-wall water tunnel facilities. *Experimental Thermal and Fluid Science* 88, 519 – 529.

Shi, W., G. Zhang and D. Zhang (2014). Investigation of unsteady cavitation around hydrofoil based on PANS model. *Journal of Huazhong University of Science and Technology (Natural Science Edition)* 42(4).

Yang, D. D., A. Yu, B. Ji, J. J. Zhou and X. W. Luo (2018, April). Numerical analyses of ventilated cavitation over a 2-D NACA0015 hydrofoil using two turbulence modeling methods. *Journal of Hydrodynamics* 30, 345–356.

Yu, A., X. Luo and B. Ji (2015). Analysis of ventilated cavitation around a cylinder vehicle with nature cavitation using a new simulation method. *Science Bulletin* 60(21), 1833–1839.

Yu, A., X. Luo, D. Yang and J. Zhou (2018). Experimental and numerical study of ventilation cavitation around a naca0015 hydro-foil with special emphasis on bubble evolution and air-vapor interactions. *Engineering Computations* 35(3), 1528–1542.